A Compact Planar Four-port MIMO Antenna for 28/38 GHz Millimeter-wave 5G Applications

Abdulaziz Dessalew Tadesse, Om Prakash Acharya, and Sudhakar Sahu

School of Electronics Engineering, Kalinga Institute of Industrial Technology (KIIT), Bhubaneswar, Odisha-751024, India

Corresponding author: Om Prakash Acharya(omprakash.acharyafet@kiit.ac.in).

ABSTRACT This article presents a planar four-port microstrip line-fed Multiple-Input Multiple-Output (MIMO) antenna operating at 5G millimeter-wave candidate bands of 28 GHz and 38 GHz. A rectangular-shaped patch antenna is designed as a main radiator to obtain a resonance at 28 GHz. Etching of a single-element split-ring resonator (SRR) metamaterial unit cell from the basic patch radiator introduces an additional resonance band at 38 GHz. The suggested MIMO antenna is built on Rogers RT5880 substrate material with a dimension of 14 mm × 14 mm, a thickness of 0.8 mm, and a relative permittivity of 2.2. The measured results show that the antenna achieves bandwidths of 26.6-29 GHz and 37.3-39.3 GHz, whereas greater than 25 dB of port isolation between antenna elements over both bands is obtained without applying any complex decoupling structure. The antenna's equivalent circuit diagram is presented with the help of lumped elements to characterize its electrical responses. The investigated diversity performance parameters, which result in an envelope correlation coefficient below 0.005, diversity gain of almost 10 dB, and channel capacity loss of less than 0.35 bits/s/Hz, are all found within their conventional limits. The findings show the viability of the design for millimeter-wave 5G applications.

INDEX TERMS Four-port, Metamaterial, Millimeter-wave, MIMO antenna, 5G.

I. INTRODUCTION

WITH wireless technologies rapid development, mobile communication has become linked to every aspect of life, resulting in bandwidth shortages and high data traffic. To avoid spectrum scarcity in microwave bands and to realize high data rate and bandwidth requirements, the FCC assigned the millimeter-wave frequency range of 25-70 GHz to fifth-generation (5G) technologies [1]. Allocation of this broad frequency range attracted considerable interest from 5G antenna designers to develop compact and multiple antennas within a limited space. However, electromagnetic waves at millimeter-wave regions face substantial weather condition influences, such as patch loss attenuations, signal fading, and atmospheric absorptions. These effects become more prominent in systems with a single antenna [2], [3]. Assimilation of modern technologies, including multiple-input-multiple-output (MIMO), has been among the encouraging methods for present and forthcoming wireless systems to improve the transmission quality [4]. In MIMO systems, several antenna radiators are positioned at the wireless system ends to obtain polarization and spatial diversity, which in turn helps to improve channel capacity and data rate without an extra spectral frequency [5]–[7].

5G MIMO antennas having wider impedance bandwidth and high gain features are highly demanded for simultaneous operation of different services and to decrease atmospheric effects such as rain attenuation and absorption at millimeter-wave frequencies [8]. In addition, such antennas should have small dimensions and minimal mutual coupling for better diversity performance. Numerous methods have been implemented for mutual coupling reduction in millimeter-wave MIMO [9]–[18].

Recent studies in the area of 5G millimeter-wave show that wideband and multiband MIMO antennas receive significant attention [19]. A number of wideband MIMO antennas are presented in [20]–[29]. In recent research, more emphasis has been given to the development of dual-band MIMO antennas working in frequency bands extending from 25-60 GHz, mostly at 28 GHz and 38 GHz, where rain attenuation and atmospheric absorption have little influence on electromagnetic wave propagation [30].

A review of existing literature shows that the research in these millimeter-wave frequency ranges is still reasonably new. However, several dual-band MIMO antennas have been proposed [19], [31]–[36]. A planar two-element MIMO antenna presented in [19] provides resonances at 27 GHz and

39 GHz. In [31] , the antenna working at 28 GHz and 38 GHz is generated by two orthogonally placed and laterally tapered planar radiating elements. The MIMO antenna reported in [32] is designed by slotting two patches for 28 GHz and 38 GHz operation. The work of [33] also introduces two and four-element patch slotted MIMO antennas operating at these bands. The 2×2 MIMO antenna presented in [34] operates at 24 GHz and 28.5 GHz millimeter-wave frequencies. Dual-band is achieved using half-slotted stack resonators. A two-port MIMO antenna is reported in [35] and operates at 28 GHz and 38 GHz frequencies. Round-shaped double-sided electromagnetic band-gap structures are integrated inside the substrate to decrease the mutual coupling as well as improve the gain. The four-element antenna with H-shaped slots on the patches is presented in [36] for dual-band operation. The antennas are printed on the substrate and arranged orthogonally to reduce mutual coupling without using conventional decoupling mechanisms.

A four-port MIMO antenna working at both 28 GHz and 38 GHz millimeter-wave spectrums is presented in this study. The presented antenna has multiple important features mentioned below, making it a possible candidate for the 5G RF antenna system.

(1) Planar geometry, simple design, and easy to fabricate
(2) Compact size to be integrated inside 5G devices
(3) High isolation without applying any complex decoupling structure among the antenna elements
(4) Printed on a common ground plane, which is a misused practice by many authors [37]
(5) Equivalent circuit model to assess its electrical behaviour in response to an RF signal input

This paper is organized into three main sections. The proposed MIMO antenna design stages and equivalent circuit model extraction are explained in Section 2. Section 3 provides detailed discussions on the simulated and measured scattering parameters, radiation characteristics, and diversity performance results. Finally, Section 4 draws a conclusion.

II. ANTENNA DESIGN AND GEOMETRY

During the antenna design process, three main stages are accomplished. First, a single-element patch antenna has been developed for 28 GHz operation. Second, to get the second working band at 38 GHz, an SRR metamaterial unit cell is scraped from the patch. Thus, the resulting antenna works at 28 GHz and 38 GHz frequencies. Finally, using the developed antenna in stage 2 as a constituting antenna, a four-element dual-band MIMO antenna is printed on Rogers RT 5880 substrate with a size of 14 mm × 14 mm, a relative permittivity of 2.2, a dielectric loss tangent of 0.0009, and thickness of 0.8 mm. Copper material of 0.035 mm thickness is utilized to construct the main radiator elements and ground plane. The three design stages are displayed in Fig. 1, and the antennas' dimensional details are given in Table I. The suggested antenna is designed and simulated using the HFSS Software, which is commercially accessible. Also, a circuit model equivalent to the presented MIMO antenna is extracted. The next subsection provides a detailed explanation of the three design stages.

A. SINGLE-ELEMENT ANTENNA

1) PATCH ANTENNA

At the first stage, the basic patch antenna having a microstrip feed line is considered as depicted in Fig. 1(a), with the aim of getting resonance at 28 GHz using the mathematical equations (1)-(4) established in [38].

$$W_P = \frac{1}{2f_r\sqrt{\mu_0\varepsilon_r}}\sqrt{\frac{2}{\varepsilon_r+1}} = \frac{c}{2f_r}\sqrt{\frac{2}{\varepsilon_r+1}} \tag{1}$$

$$\varepsilon_{reff} = \frac{\varepsilon_r+1}{2} + \frac{\varepsilon_r-1}{2}\left(\frac{1}{\sqrt{1+12\frac{h}{W_P}}}\right) \tag{2}$$

$$\Delta L = 0.421h\frac{\left(\varepsilon_{reff}+0.3\right)\left(\frac{W_P}{h}+0.264\right)}{\left(\varepsilon_{reff}-0.258\right)\left(\frac{W_P}{h}+0.8\right)} \tag{3}$$

$$L_P = \frac{c}{2f_r\sqrt{\varepsilon_{reff}}} - 2\Delta L \tag{4}$$

where W_P represents width and L_P represents length of the patch, whereas h, ε_r and ε_{reff} are the substrate material height, relative permittivity, and effective permittivity, respectively. The other parameters like ΔL, c, and f_r correspondingly denote the effective length, speed of light, and resonance frequency. This initially designed conventional patch antenna generated a broad operational frequency range of 26.4-29.4 GHz, centered at 27.9 GHz.

2) PATCH ANTENNA WITH CSRR

The designed basic antenna is further upgraded to create additional resonance at 38 GHz millimeter-wave frequency. For this purpose, a rectangular-shaped singly-ring complementary SRR (CSRR) having high transmission and low reflection characteristics at the intended frequency is initially designed and then loaded onto the main radiating patch as depicted in Fig. 1(b). The simulation results of Fig. 4(a) show the two resonance bands of this antenna, extending from 26.4-29 GHz and 36.9-39.1 GHz.

B. MIMO ANTENNA

After the achievement of the constituting antenna element, the design is evolved to obtain the dual-band MIMO antenna. As displayed in Fig. 1(c), the constituting four antennas are positioned orthogonally with a spacing of 'd' units. This

orthogonal arrangement would enable polarization diversity and could be utilized to further lessen the mutual coupling created between different antenna components [31] without applying any complex decoupling structure. The board has a 14 mm × 14 mm total dimension.

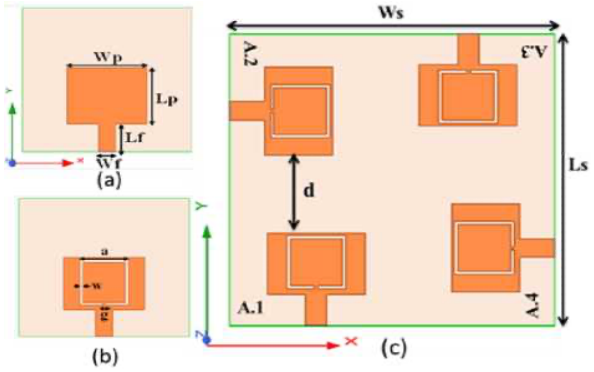

FIGURE 1. The proposed MIMO antenna development stages: (a) patch antenna, (b) patch antenna with CSRR, and (c) final MIMO geometry.

TABLE I. The single and proposed MIMO antenna parameters and their values (unit: mm)

Parameter	Wp	Lp	Wf	Lf	a
Value(mm)	4.23	2.94	0.9	1.5	2.55
Parameter	w	g	Ws	Ls	d
Value(mm)	0.15	0.15	14	14	3.72

C. EQUIVALENT CIRCUIT DIAGRAM

This section highlights the proposed four-port MIMO antenna lumped-circuit model to evaluate its electrical behaviour in response to an input RF signal. The modelling, execution, and optimization of the corresponding circuit are performed using Advanced Design System (ADS) electromagnetic simulation tool. The complete circuit consists of five blocks representing the four antennas (A.1, A.2, A.3, and A.4) and the coupling section as presented in Fig. 2. During the circuit element extraction procedure, the input impedance is initially generated using the HFSS antenna design tool. From the input impedance graph, the lumped RLC components are extracted and then exported in ADS with the details mentioned in [11], [39]. In the dual-band operation of antenna 1 (A.1), for example, the PRLC1 and PRLC2 represent the lower and upper-frequency bands, whereas C12 and L12 represent the mutual coupling between A.1 and A.2.

Parametric tuning is performed in ADS to obtain better component values whose responses match the HFSS simulated ones. The corresponding circuit element values are provided in Table II. The scattering parameters of the MIMO antenna obtained from HFSS simulation and ADS equivalent circuit model responses are displayed in Fig. 3. As can be observed, the results have a reasonable agreement between them for the two operation bands.

TABLE II. Lumped element parametric values of the equivalent circuit diagram

Element	Value	Element	Value	Element	Value
Ri (i=1,2,3,4)	9.6 Ω	C13	2.005pF	C23	4.7pF
Ci (i=1,2,3,4)	1.086 pF	L13	1.87nH	L23	11.6nH
Li (i=1,2,3,4)	7.44 pH	C14	4.7pF	C24	2.46pF
C12	3pF	L14	11.6nH	L24	2.075nH
L12	1.665nH	C34	11.4pF	L34	1.8nH
PRLC(1,3,6,7)			PRLC(2,4,5,8)		
R	46.77Ω	L	21.318pH	R	45.896Ω	L	24.96pH
C	1.61 pF			C	0.7059pF		

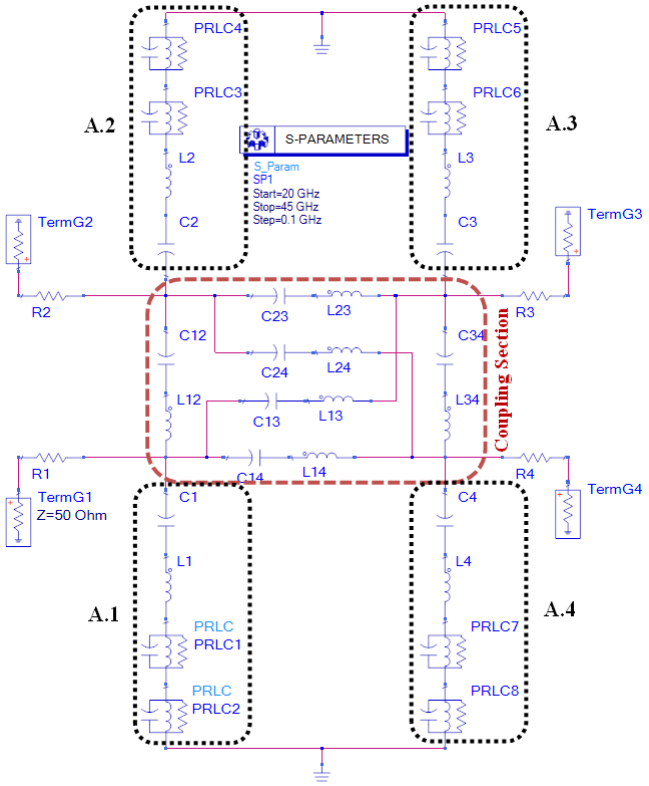

FIGURE 2. Equivalent circuit diagram of the MIMO antenna plotted using ADS.

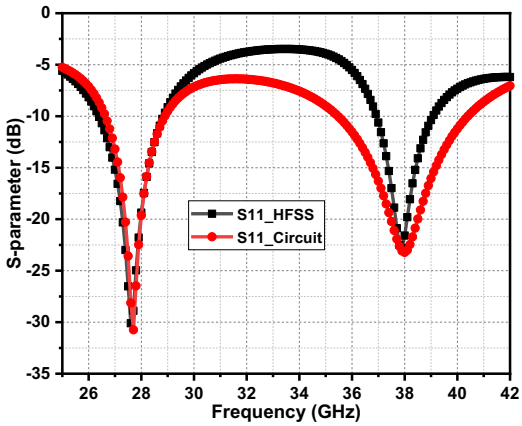

(a)

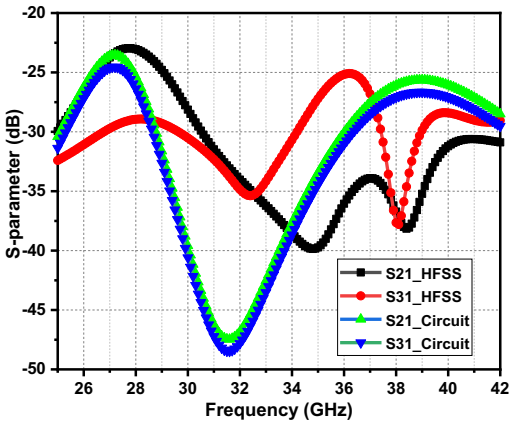

(b)

FIGURE 3. S-parameters comparison of HFSS and ADS circuit models: (a) reflection and (b) transmission coefficients.

III. RESULTS AND DISCUSSION

The MIMO antenna performances are analysed by means of scattering parameters, surface current distribution, radiation characteristics, and diversity performance metrics.

A. S-PARAMETERS

Fig.4 demonstrates the reflection and transmission parameters of the patch antenna without and with the application of CSRR. As presented in Fig. 4(a), prior to the introduction of the CSRR structure, the antenna resonates at 28 GHz, whereas the CSRR loading creates additional resonance at 38 GHz. To verify that the 38 GHz band is created owing to CSRR loading, parametric analysis is performed on the length (a) of the CSRR structure by keeping its slit gap (g) and slot width (w) constant for simplicity purposes. The CSRR length is made to vary from 2.4 mm to 2.6 mm, and resonance with better impedance matching is achieved at 38 GHz when the length becomes 2.55 mm, as displayed in Fig. 4(b). As can be noted, the variation of CSRR length offers independent tunability at the higher band without any impact on the primary lower band.

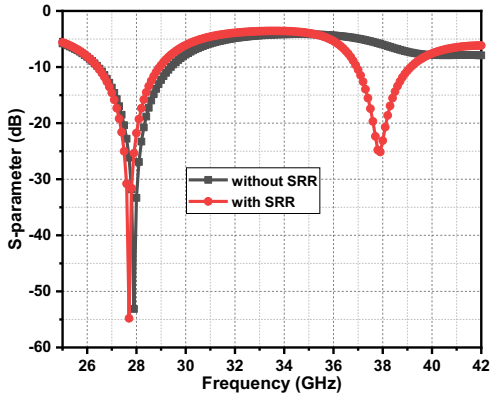

(a)

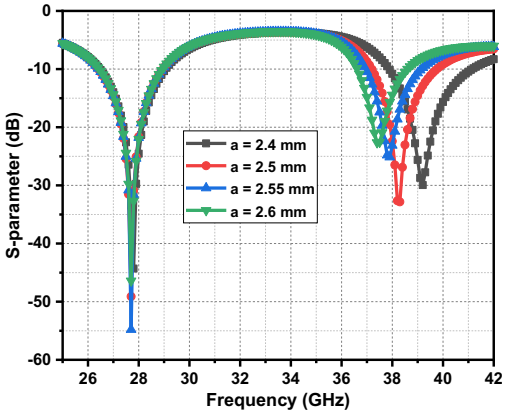

(b)

Figure 4. The single antenna reflection coefficient: (a) without/with CSRR and (b) variation of CSRR arm length (a).

For the analysis of the CSRR structure in the HFSS tool, a conventional waveguide setup is applied [40]. The effective permittivity of CSRR is extracted from the reflection and transmission parameters using equations (5)-(7) as proposed by [41].

$$n = \frac{1}{kd}\cos^{-1}\left[\frac{1}{2S_{21}}\left(1 - S^2_{11} + S^2_{21}\right)\right] \tag{5}$$

$$z = \sqrt{\frac{\left(1+S_{11}\right)^2 - S^2_{21}}{\left(1-S_{11}\right)^2 - S^2_{21}}} \tag{6}$$

$$\varepsilon = \frac{n}{z} \tag{7}$$

where n, z, and ε are the refractive index, wave impedance, and effective permittivity of the CSRR respectively.

Fig. 5 shows the CSRR scattering characteristics and its metamaterial property. Fig. 5(a) depicts the passband region, whereas Fig. 5(b) indicates the negative permittivity response of the CSRR structure for the creation of the second resonance at 38 GHz.

The fabricated MIMO antenna is depicted in Fig. 6, and S-parameters measurement is executed using the PNA-X network analyser. Since the four antenna elements are identical and symmetrically arranged, excitation is given to only one port during the measurement, whereas the others are terminated with 50Ω loads.

Fig. 7 displays simulated and measured S-parameters of the MIMO antenna. The antenna has resonances at 28 GHz and 38 GHz, as given in Fig. 7(a), with simulated impedance bandwidths of 9.42% (26.3-28.9 GHz) and 5.77% (37-39.2 GHz), and measured bandwidths of 8.63% (26.6-29 GHz)

and 5.22% (37.3-39.3 GHz). Measured and simulated results correspond well with a slight shift in frequency that occurs as a result of losses in cables and fabrication faults. To further evaluate the coupling between elements, the MIMO antenna isolation results are presented in Fig. 7(b). As illustrated, a measured isolation value of more than 25 dB is realized at both bands.

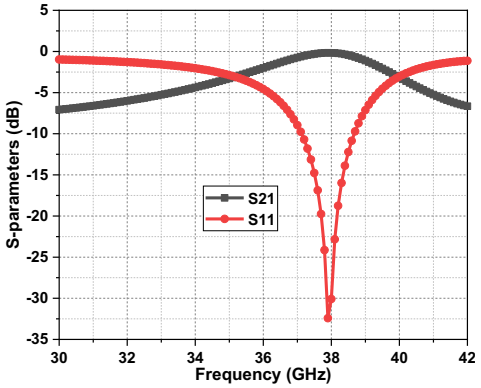

(a)

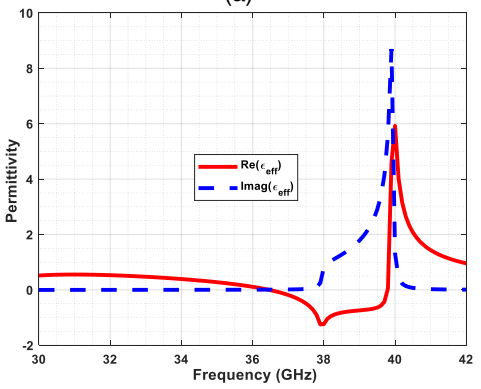

(b)

FIGURE 5. The CSRR unit cell: (a) S-parameters and (b) permittivity parameter.

(a) (b)

FIGURE 6. (a) Top view and (b) bottom view of the fabricated MIMO antenna.

B. CURRENT DISTRIBUTION

To further explore the MIMO antenna's radiation mechanism, the current distributions on the surface of the patches at 28 GHz and 38 GHz frequencies are displayed in Fig. 8. As shown, the surface current predominantly distributes on the patch radiator at 28 GHz, whereas more current concentration is seen at the upper portion of the SRR unit at 38 GHz frequency.

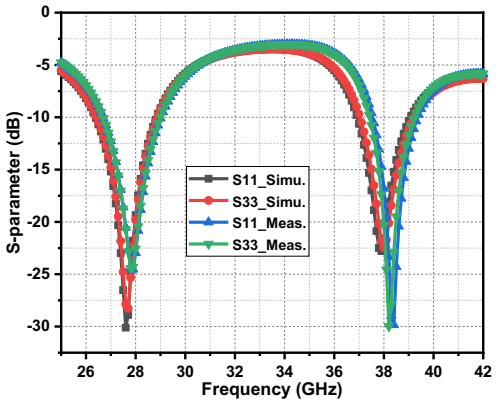

(a)

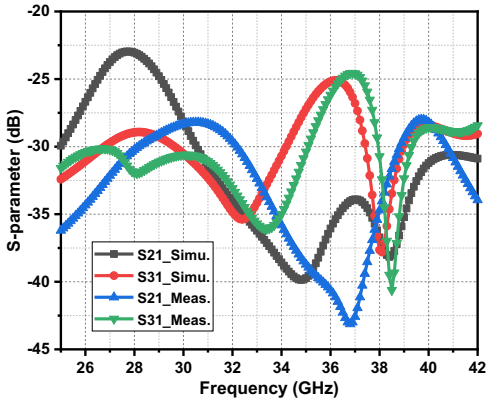

(b)

FIGURE 7. The MIMO antenna (a) reflection and (b) transmission parameters.

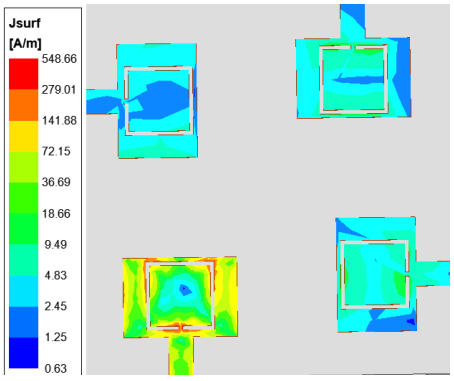

(a)

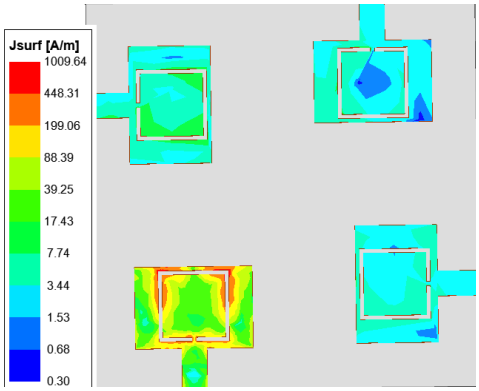

(b)

FIGURE 8. The proposed MIMO antenna current distribution at (a) 28 GHz and (b) 38 GHz.

C. RADIATION PATTERN

The simulated 2D-far-field radiation patterns are shown in Fig. 9 to realize the radiation performance of the presented MIMO antenna. The E-plane (xz-plane) and Y-plane (yz-plane) far-field radiation patterns are plotted at 28 GHz and 38 GHz.

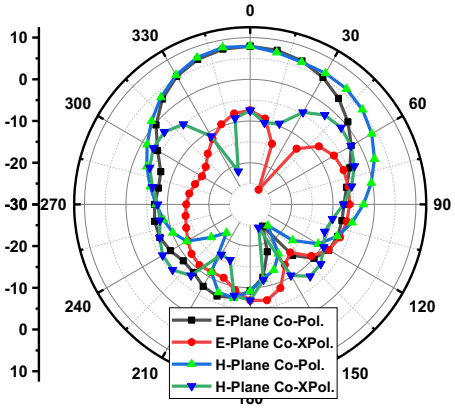

(a)

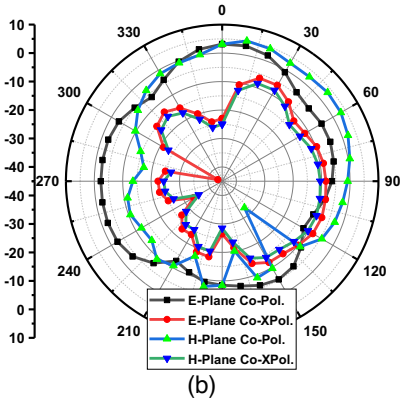

(b)

FIGURE 9. The proposed MIMO antenna radiation patterns at (a) 28 GHz and (b) 38 GHz.

D. GAIN AND RADIATION EFFICIENCY

Fig. 10 displays the MIMO antenna's simulated gain and radiation efficiency. As depicted in the figure, the antenna has gains of 8.4 dB at 28 GHz and 6.02 dB at 38 GHz with respective efficiencies of 91.66% and 88.57%. The 3D radiation patterns at these operating frequencies are revealed in Fig. 11 to further validate the radiation characteristics and gain results.

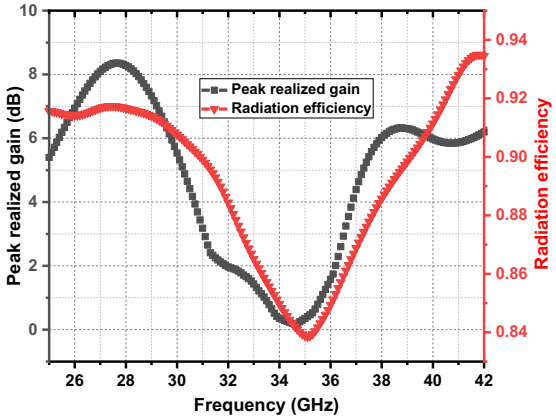

FIGURE 10. The MIMO antenna gain and radiation efficiency.

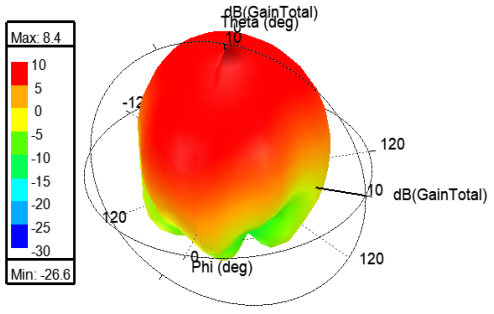

(a)

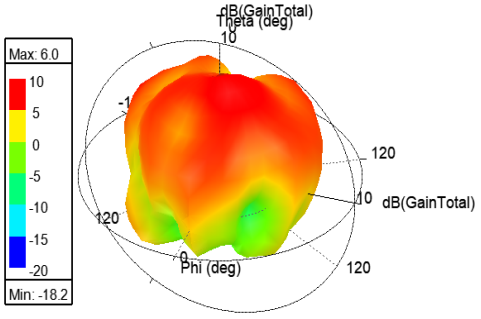

(b)

FIGURE 11. The MIMO antenna 3D radiation patterns (a) 28 GHz and (b) 38 GHz.

E. MIMO PERFORMANCE PARAMETERS

This section presents the envelope correlation coefficient (ECC), diversity gain (DG), mean effective gain (MEG), effective diversity gain (EDG) and channel capacity loss

(CCL) diversity performance results using a written MATLAB code.

1) ECC AND DG

ECC is among the important MIMO performance metrics associated with the correlation between two concurrently operating and closely positioned antenna elements. The parameter can be computed using far-field radiation patterns or S-parameters of the ith and jth antennas as mathematically given in equations (8) and (9) [5], [42].

$$ECC = \frac{\left| \iint_{4\pi} \left(\overrightarrow{F_i}(\theta,\phi) \times \overrightarrow{F_j}^{*}(\theta,\phi) \right) d\Omega \right|^2}{\iint_{4\pi} \left| \left(\overrightarrow{F_i}(\theta,\phi) \right) \right|^2 d\Omega \times \iint_{4\pi} \left| \left(\overrightarrow{F_j}(\theta,\phi) \right) \right|^2 d\Omega} \quad (8)$$

where $F_i(\theta,\phi)$ and $F_j(\theta,\phi)$ are the ith and jth antennas' far field radiation patterns.

$$ECC = \frac{\left| S^*_{ii} S_{ij} + S^*_{ji} S_{jj} \right|^2}{\left(1 - \left(|S_{ii}|^2 + |S_{ji}|^2 \right)\right) + \left(1 - \left(|S_{jj}|^2 + |S_{ij}|^2 \right)\right)} \quad (9)$$

where S_{ii} and S_{ij} denotes the reflection and transmission coefficients.

DG is another parameter that defines the reduction in transmission power or signal-to-noise ratio improvement due to the diversity system. Mathematically, DG is computed from ECC values using equation (10)[43].

$$DG = 10\sqrt{1 - (ECC)^2} \quad (10)$$

The ECC and DG values between a set of antenna elements are presented in Fig. 12(a) and 12(b). The simulated (from simulated radiation patterns) and measured (from measured S-parameters) results show a very low ECC value below 0.005, satisfying the ECC < 0.5 criterion [44], along with DG values much closer to 10 dB for both working bands, providing good antenna diversity performance.

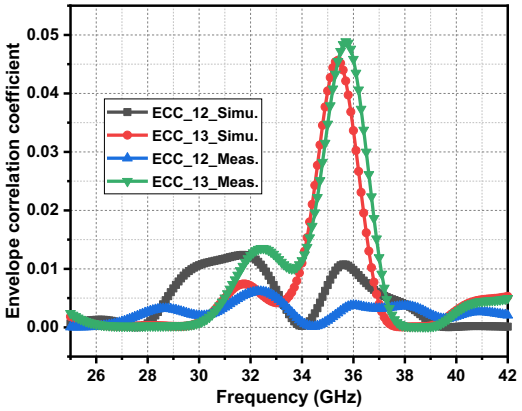

(a)

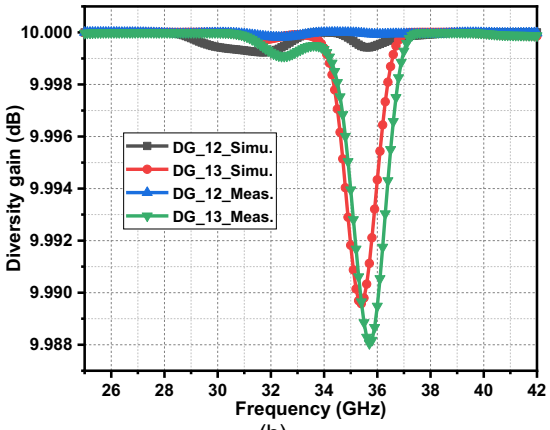

(b)

FIGURE 12. The proposed MIMO antenna (a) ECC and (b) DG.

2) MEG AND EDG

MEG is the ratio of the accepted mean power to the average incident power by the antenna in comparison to the isotropic antenna. It can be calculated using the relation given in [45].The simulated and measured results are shown in Fig. 13.It can be seen that the antennas possess good values of MEG in the range from -0.4 dB to 0.4 dB.

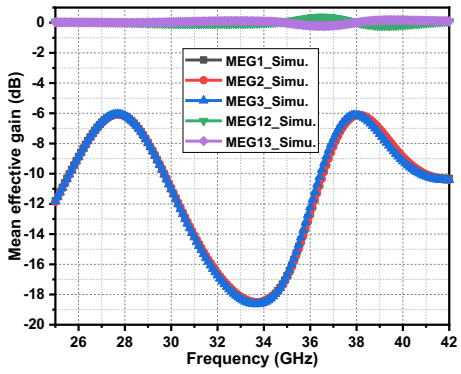

(a)

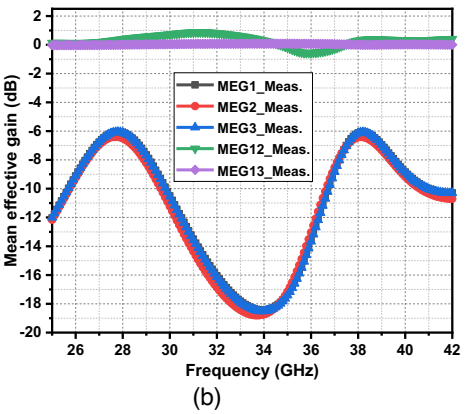

(b)

FIGURE 13. The proposed MIMO antenna MEG (a) Simulated and (b) measured.

EDG of the multi-antenna system provides the lower bound for diversity gain performance. Mathematically, it can be computed from the radiation efficiency and diversity gain using the relation given in equation (11) [46]. For the

proposed MIMO antenna, the EDG is given in Fig. 14.The figure shows that the antenna achieves EDG values of greater than 9 dB and 8.7 dB at the two operating bands, respectively.

$$EDG = \eta_{rad} \times DG \qquad (11)$$

where η_{rad} and DG represent the radiation efficiency and the diversity gain, respectively.

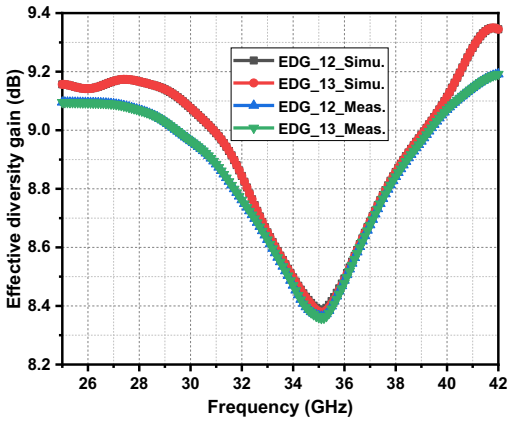

FIGURE 14. The EDG of the proposed MIMO antenna.

3) CHANNEL CAPACITY LOSS

CCL provides the system channel capacity losses caused by the correlation effect of the multiple antennas. Mathematically, it can be calculated using equation (12) and should be below 0.4 bits/s/Hz standard limit over the working bands [47].

$$C_{loss} = -\log_2 \det\left(\alpha^R\right) \qquad (12)$$

where

$$\alpha^R = \begin{pmatrix} \alpha_{11} & \alpha_{12} \\ \alpha_{21} & \alpha_{22} \end{pmatrix}$$

$$\alpha_{ii} = 1 - \sum_{j=1}^{N} \left|S_{ij}\right|^2 \text{, and}$$

$$\alpha_{ij} = -\left(S^*_{ii} S_{ij} + S^*_{ji} S_{ij}\right)$$

As depicted in Fig. 15, a CCL value of not more than 0.35 bits/s/Hz is obtained for the two bands, indicating the MIMO channel reliability.

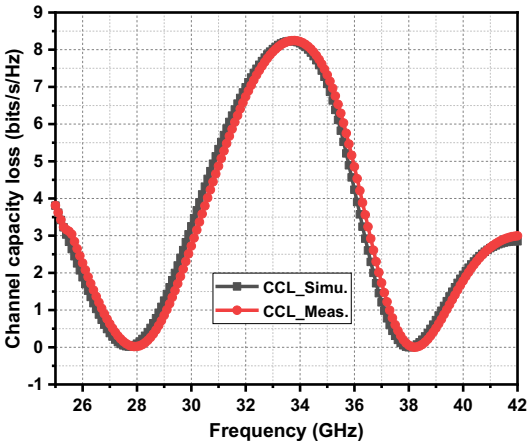

FIGURE 15. The CCL of the proposed MIMO antenna.

TABLE III. Comparison between different dual-band MIMO antenna performances reviewed in literature

Ref.	Ant.	TA (mm^2)	Bands	Bandwidth (GHz)	I_{min} (dB)	AP/ GP
[19]	2	26 x 11 4.01λg x 1.73λg	27/39	25–29/ 37-41	30/25	✓/×
[31]	2	14 x 26 1.84λg x 3.43λg	28/38	26.65-29.2/ 36.95-39.05	20	✓/×
[32]	2	NP	28/38	NP	25/30	✓/☑
[33]	4	55 x 110 NP	28/38	NP	26	✓/×
[34]	4	NP	24/28.5	23.47-25 /27.2-31.7	30	▦/ ☑
[35]	2	15.3 x 8.5 NP	28/38	27-29/ 35-40	NP	☒/☑
[36]	4	20 x 24 2.73λg x 3.28λg	28/38	27.6-28.6/ 37.4-38.6	28	✓/☑
This work	4	14 x 14 1.82λg x 1.82λg	28/38	26.6-29/ 37.3-39.3	25	✓/☑

TABLE IV. Comparison of MIMO performance parameters of the proposed MIMO antenna with the dual-band MIMO antenna mentioned in Table III

Ref.	Gain (dBi)	Efficiency (%)	ECC	DG (dB)	MEG (dB)	CCL (bits/s/ Hz)
[19]	5/5.7	99.5/98.6	0.0001	Near 10	NP	NP
[31]	1.27 /1.83	78/76	0.001	Near 10	NP	Below 0.4
[32]	5.2/5	84/91	0.001	NP	NP	NP
[33]	7.95/8.27	89.9/88.3	7.65×10-5	NP	NP	NP
[34]	3.5/4	92/95	NP	NP	NP	NP
[35]	6.19/ 7.16	87.6/ 90.1	0.01	Near 10	-0.29/ -0.21	NP
[36]	7.9	85	0.001	NP	NP	NP
This work	8.4/ 6.02	91.7/ 88.6	0.005	Near 10	-0.4 to 0.4	0.35

Key: TA = Total area of the antenna, λg = guided wavelength at the lowest operation frequency (fL), I_{min} = minimum isolation for band 1 and band 2," NP " = not provided, AP/GP = antenna profile(✓= planar, ▦=stack, ☒=via)/ground plane (☑=common, × = separate).

Table III and IV compare the performances of this suggested MIMO antenna to recently reported dual-band MIMO antennas anticipated for potential 5G applications.The comparison with previous works reveals that the proposed antenna has a very small dimension and comparable isolation without deploying a decoupling structure.This planar geometry MIMO antenna is also backed with an inter-connected ground plane in contrast to the works in [19], [31], [33].Moreover, the antenna in [34] uses a substrate layer approach that poses difficulties for integration into wireless devices.The work also gives several MIMO performance parameter results for a more thorough investigation of the antenna's diversity performance, which the comparable works failed to provide.From the comparison, one can reach the conclusion that the proposed MIMO antenna delivers the above-mentioned antenna features and better performances required for the contemporary portable devices pointing towards 5G millimeter-wave wireless communications.

IV. CONCLUSION

A four-port dual-band metamaterial-inspired MIMO antenna is proposed in this work for applications at 28 GHz and 38 GHz millimeter-wave bands.The antenna achieves a measured port isolation of more than 25 dB without any decoupling structure in a shared ground plane configuration. It also attains acceptable antenna gains at both frequency bands with desirable ECC and CCL diversity performance values. Moreover, the presented planar and 14 mm × 14 mm sized compact MIMO antenna can be appropriate for integration into multiple 5G wireless devices.

REFERENCES

[1] N. Al-falahy and O. Y. K. Alani, "Millimetre wave frequency band as a candidate spectrum for 5G network architecture : A survey," *Phys. Commun.*, vol. 32, pp. 120–144, 2019.

[2] J. Zhang, X. Ge, Q. Li, M. Guizani, and Y. Zhang, "5G millimeter-wave antenna array: Design and challenges," *IEEE Wirel. Commun.*, vol. 24, no. 2, pp. 106–112, 2017.

[3] I. Shayea, T. A. Rahman, M. H. Azmi, and R. Islam, "Real Measurement Study for Rain Rate and Rain Attenuation Conducted Over 26 GHz Microwave 5G Link System in Malaysia," *IEEE Access*, vol. 6, pp. 19044–19064, 2018.

[4] S. A. Busari, S. Mumtaz, S. Al-rubaye, and J. Rodriguez, "5G Millimeter-Wave Mobile Broadband : Performance and Challenges," *IEEE Commun. Mag.*, vol. 56, no. 6, pp. 137–143, 2018.

[5] M. S. Sharawi, "Printed multi-band MIMO antenna systems and their performance metrics," *IEEE Antennas Propag. Mag.*, vol. 55, no. 5, pp. 218–232, 2013.

[6] P. R. Girjashankar and T. Upadhyaya, "Substrate integrated waveguide fed dual band quad-elements rectangular dielectric resonator MIMO antenna for millimeter wave 5G wireless communication systems," *AEU- Int. J. Electron. Commun.*, vol. 137, 2021.

[7] N. O. Parchin, A. Basherlou, H.J., M., (...), R. A. Abd-Alhameed, and E. Limiti, "Mobile-Phone Antenna Array with Diamond-Ring Slot Elements for 5G Massive MIMO Systems," *Electronics*, vol. 8, no. 5, 2019.

[8] Z. Qingling and J. Li, "Rain Attenuation in Millimeter Wave Ranges," in *International Symposium on Antennas, Propagation & EM Theory*, 2006, pp. 1–4.

[9] A. Iqbal *et al.*, "Electromagnetic bandgap backed millimeter-wave MIMO antenna for wearable applications," *IEEE Access*, vol. 7, pp. 111135–111144, 2019.

[10] Y. Zhang, J. Deng, M. Li, and D. Sun, "A MIMO Dielectric Resonator Antenna With Improved Isolation for 5G mm-Wave Applications," *IEEE Antennas Wirel. Propag. Lett.*, vol. 18, no. 4, pp. 747–751, 2019.

[11] R. Selvaraju, M. H. Jamaluddin, M. R. Kamarudin, J. Nasir, and M. H. Dahri, "Complementary Split Ring Resonator for Isolation Enhancement in 5G Communication Antenna Array," *Prog. Electromagn. Res. C*, vol. 83, pp. 217–228, 2018.

[12] Z. Wani, M. P. Abegaonkar, and S. K. Koul, "A 28-GHz Antenna for 5G MIMO Applications," *Prog. Electromagn. Res. Lett.*, vol. 78, pp. 73–79, 2018.

[13] H. Ullah and F. A. Tahir, "A wide-band rhombus monopole antenna array for millimeter wave applications," *Microw. Opt. Technol. Lett.*, vol. 62, no. 5, pp. 2111–2117, 2020.

[14] Y. Usha Devi, B. T. p. Madhav, T. Anil Kumar, K. C. Sri Kavya, and P. Pardhasaradhi, "Conformal printed MIMO antenna with DGS for millimetre wave communication applications," *Int. J. Electron. Lett.*, vol. 8, no. 3, pp. 329–343, 2019.

[15] K. Gulur Sadananda, M. P. Abegaonkar, and S. K. Koul, "Gain Equalized Shared-Aperture Antenna Using Dual-Polarized ZIM for mmWave 5G Base Stations," *IEEE Antennas Wirel. Propag. Lett.*, vol. 18, no. 6, pp. 1100–1104, 2019.

[16] A. Abdelaziz and E. K. Hamad, "Isolation enhancement of 5G multiple-input multiple- output microstrip patch antenna using metamaterials and the theory of characteristic modes," *Int. J. RF Microw. Comput. Eng.*, vol. 30, no. 11, 2020.

[17] M. Usman and et al., "Compact SIW Fed Dual-Port Single Element Annular Slot MIMO Antenna for 5G mmWave Applications," *IEEE Access*, vol. 9, pp. 91995–92002, 2021.

[18] Z. Xu, Q. Zhang, and L. Guo, "A printed multiband MIMO antenna with decoupling element," *Int. J. Microw. Wirel. Technol.*, vol. 11, no. 4, pp. 413–419, 2019.

[19] W. Ali, S. Das, H. Medkour, and S. Lakrit, "Planar dual-band 27 / 39 GHz millimeter-wave MIMO antenna for 5G applications," *Microsyst. Technol.*, vol. 27, no. 1, pp. 283–292, 2020.

[20] M. Khalid *et al.*, "4-port MIMO antenna with defected ground structure for 5G millimeter wave applications," *Electron.*, vol. 9, no. 1, 2020.

[21] N. Hussain, M. J. Jeong, J. Park, and N. A. M. Kim, "A Broadband Circularly Polarized Fabry-Perot Resonant Antenna Using A Single-Layered PRS for 5G MIMO Applications," *IEEE Access*, vol. 7, pp. 42897–42907, 2019.

[22] A. A. R. Saad and H. A. Mohamed, "Printed millimeter-wave MIMO-based slot antenna arrays for 5G networks," *AEU - Int. J. Electron. Commun.*, vol. 99, pp. 59–69, 2019.

[23] S. F. Jilani and A. Alomainy, "Millimetre-wave T-shaped MIMO antenna with defected ground structures for 5G cellular networks," *IET Microwaves, Antennas Propag.*, vol. 12, no. 5, pp. 672–677, 2018.

[24] M. Ikram, A. Shamim, and M. S. Sharawi, "A switched-beam millimeter- wave array with MIMO configuration for 5G applications," *Microw. Opt. Technol. Lett.*, vol. 60, no. 4, pp. 915–920, 2018.

[25] N. Shoaib, S. Shoaib, R. Y. Khattak, I. Shoaib, X. Chen, and A. Perwaiz, "MIMO Antennas for Smart 5G Devices," *IEEE Access*, vol. 6, pp. 77014–77021, 2018.

[26] R. Selvaraju, M. H. Jamaluddin, M. R. Kamarudin, J. Nasir, and M. H. Dahri, "Mutual Coupling Reduction and Pattern Error Correction in a 5G Beamforming Linear Array Using CSRR," *IEEE Access*, vol. 6, pp. 65922–65934, 2018.

[27] X. Shen, Y. Liu, L. Zhao, G. L. Huang, X. Shi, and Q. Huang, "A Miniaturized Microstrip Antenna Array at 5G Millimeter-Wave Band," *IEEE Antennas Wirel. Propag. Lett.*, vol. 18, no. 8, pp. 1671–1675, 2019.

[28] F. Khajeh-Khalili, M. A. Honarvar, M. Naser-Moghadasi, and M. Dolatshahi, "Gain enhancement and mutual coupling reduction of multiple-intput multiple-output antenna for millimeter-wave applications using two types of novel

metamaterial structures," *Int. J. RF Microw. Comput. Eng.*, vol. 30, no. 1, 2020.

[29] Z. Wani, M. P. Abegaonkar, and S. K. Koul, "Millimeter-wave antenna with wide-scan angle radiation characteristics for MIMO applications," *Int. J. RF Microw. Comput. Eng.*, vol. 29, no. 5, 2019.

[30] T. S. Rappaport *et al.*, "Millimeter wave mobile communications for 5G cellular: It will work!," *IEEE Access*, vol. 1, pp. 335–349, 2013.

[31] N. Hasan, S. Bashir, and S. Chu, "Dual band omnidirectional millimeter wave antenna for 5G communications," *J. Electromagn. Waves Appl.*, vol. 33, no. 12, pp. 1581–1590, 2019.

[32] H. Aliakbari, A. Abdipour, A. Costanzo, D. Masotti, R. Mirzavand, and P. Mousavi, "ANN-based design of a versatile millimetre- wave slotted patch multi-antenna configuration for 5G scenarios," *IET Microwaves, Antennas Propag.*, vol. 11, no. 9, pp. 1288–1295, 2017.

[33] H. M. Marzouk, M. I. Ahmed, and A. A. Shaalan, "Novel dual-band 28/38 GHz MIMO antennas for 5g mobile applications," *Prog. Electromagn. Res. C*, vol. 93, pp. 103–117, 2019.

[34] M. Aboualalaa *et al.*, "Independent Matching Dual-Band Compact Quarter-Wave Half-Slot Antenna for Millimeter-Wave Applications," *IEEE Access*, vol. 7, pp. 130782–130790, 2019.

[35] D. T. T. Tu, N. T. B. Phuong, P. D. Son, and V. Van Yem, "Improving characteristics of 28/38GHz MIMO antenna for 5G applications by using double-side EBG structure," *J. Commun.*, vol. 14, no. 1, pp. 1–8, 2019.

[36] K. Raheel *et al.*, "E-Shaped H-Slotted Dual Band mmWave Antenna for 5G Technology," *Electron.*, vol. 10, no. 9, 2021.

[37] M. S. Sharawi, "Current Misuses and Future Prospects for Printed Multiple-Input, Multiple-Output Antenna Systems," *IEEE Antennas Propag. Mag.*, vol. 59, no. 2, pp. 162–170, 2017.

[38] C. A. Balanis, "Microstrip Antennas," in *Antenna Theory: Analysis and Design*, 3rd edn., John Wiley & Sons, 2005, pp. 769–830.

[39] J. Ghosh, S. Ghosal, D. Mitra, S. Ranjan, and B. Chaudhuri, "Mutual Coupling Reduction between Closely Placed Microstrip Patch Antenna Using Meander Line Resonator," *Prog. Electromagn. Res. Lett.*, vol. 59, pp. 115–122, 2016.

[40] V. Rajeshkumar and S. Raghavan, "A compact metamaterial inspired triple band antenna for reconfigurable WLAN / WiMAX applications," *AEU- Int. J. Electron. Commun.*, vol. 69, no. 1, pp. 274–280, 2015.

[41] D. R. Smith, D. C. Vier, T. Koschny, and C. M. Soukoulis, "Electromagnetic parameter retrieval from inhomogeneous metamaterials," *Phys. Rev. E*, vol. 71, no. 3, 2005.

[42] J. Li *et al.*, "Dual-Band Eight-Antenna Array Design for MIMO Applications in 5G Mobile Terminals," *IEEE Access*, vol. 7, pp. 71636–71644, 2019.

[43] R. Subhanrao Bhadade and S. Padmakar Mahajan, "Circularly polarized 4 × 4 MIMO antenna for WLAN applications," *Electromagnetics*, vol. 39, no. 5, pp. 325–342, 2019, doi: 10.1080/02726343.2019.1619227.

[44] D. Sipal, M. P. Abegaonkar, and S. K. Koul, "Easily Extendable Compact Planar UWB MIMO Antenna Array," *IEEE Antennas Wirel. Propag. Lett.*, vol. 16, pp. 2328–2331, 2017.

[45] T. Taga, "Analysis for Mean Effective Gain of Mobile Antennas in Land Mobile Radio Environments," *IEEE Trans. Veh. Technol.*, vol. 39, no. 2, pp. 117–131, 1990.

[46] S. R. Pasumarthi, J. B. Kamili, and M. P. Avala, "Design of dual band MIMO antenna with improved isolation," *Microw. Opt. Technol. Lett.*, vol. 61, no. 6, pp. 1579–1583, 2019.

[47] R. N. Tiwari, P. Singh, B. K. Kanaujia, and K. Srivastava, "Neutralization technique based two and four port high isolation MIMO antennas for UWB communication," *AEU - Int. J. Electron. Commun.*, vol. 110, 2019.